Available online at www.sciencedirect.com

jmr&t Journal of Materials Research and Technology

https://www.journals.elsevier.com/journal-of-materials-research-and-technology

Original Article

Humidity sensing of thin film perovskite nanostructure for improved sensitivity and optical performance

Muhammad Quisar Lokman[a,*], *Husna Mardiyah Burhanuddin*[b], *Muhammad Arif Riza*[a,c], *Nurul Nazli Rosli*[a], *Noor Hazirah Hashim*[d], *Suhaila Sepeai*[a], *Norasikin Ahmad Ludin*[a], *Mohd Asri Mat Teridi*[a], *Fauzan Ahmad*[b], *Mohd Adib Ibrahim*[a,*]

[a] *Solar Energy Research Institute, Universiti Kebangsaan Malaysia, 43600 Bangi, Selangor Darul Ehsan, Malaysia*
[b] *Malaysia-Japan International Institute of Technology, Universiti Teknologi Malaysia Kuala Lumpur, 54100 Kuala Lumpur, Malaysia*
[c] *School of Engineering & Physical Sciences, Heriot-Watt University, 62200 Putrajaya, Malaysia*
[d] *Faculty of Applied Sciences, Universiti Teknologi MARA Pahang, 26400 Bandar Jengka, Pahang Darul Makmur, Malaysia*

ARTICLE INFO

Article history:
Received 23 July 2020
Accepted 7 September 2020
Available online 2 October 2020

Keywords:
Humidity sensor
Nickel
Optical sensor
Zinc tin oxide

ABSTRACT

This paper presents a humidity sensing based on perovskites nanostructured thin film for improved sensitivity and optical performance. The nickel-doped zinc thin oxide (NZTO) perovskites thin film was used as a sensing material for the humidity sensing application. The NZTO was deposited on borosilicate glass substrates via aerosol-assisted chemical vapour deposition (AACVD) and nickel (Ni) dopant with 2 %mol was added into the precursor solution. The optical performance was investigated by inserting the NZTO into the optical reflection cavity. The cavity comprises NZTO on the glass that placed in a fixed position in front of single-mode fiber (SMF) and SMF was adjusted using x-direction of the 3-axis stage to obtained different cavity lengths. The performance was evaluated from the free-spectral range (FSR) and extinction ratio (E_R) of the different cavity lengths. Then, the cavity with an optimized length was placed inside the humidity chamber for sensing applications. The result shows that the optimized cavity length is 100 μm with FSR and E_R of 12.05 nm and 7.247 dB. The sensitivity of the humidity sensing is 0.2657 nm/RH% indicates that the NZTO is an excellent candidate for humidity sensing application.

1. Introduction

Humidity has a significant impact in various areas of applications such as agriculture, food processing, or manufacturing [1–3]. All these applications, which can affect by humidity, involve continuous monitoring of air humidity. Besides that,

* *Corresponding authors.*
E-mails: quisar@ukm.edu.my (M.Q. Lokman), mdadib@ukm.edu.my (M.A. Ibrahim).
https://doi.org/10.1016/j.jmrt.2020.09.036

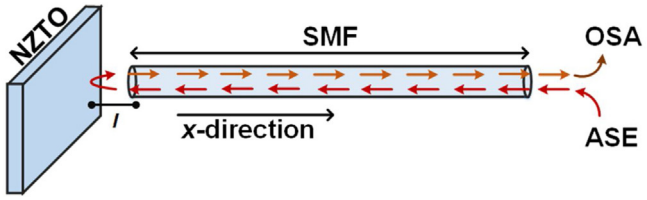

(a)

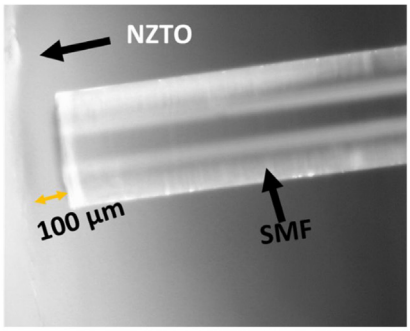

(b)

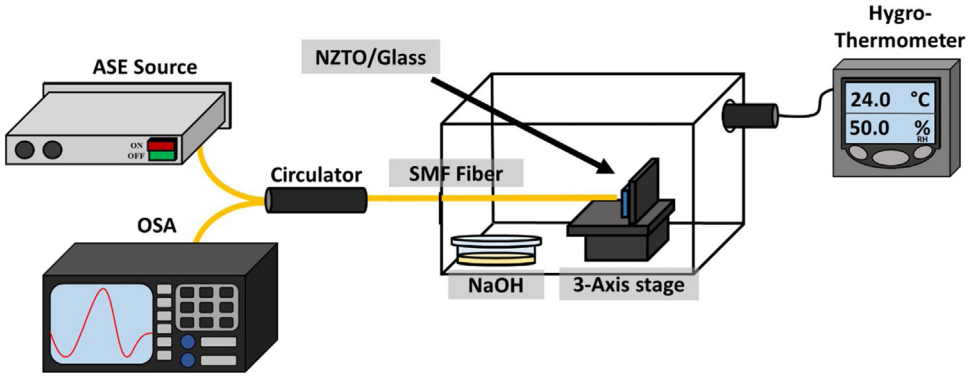

(c)

Fig. 1 – Experimental setup for optical reflection cavity (a) schematic view (b) under microscope image and (c) for humidity sensing.

suitable humidity levels can be critical to the quality of the product, and having the exact humidity level can contribute to reducing energy consumption [4]. Optical humidity sensor provides several advantages over electronic humidity sensor such as compact, durability, suitability operates on flammable environments and at elevated temperature, and immune to electromagnetic interferences. Thus, they can sustain the kind of harsh and demanding conditions in the industrial area. Typically, an optical humidity sensor requires moisture-sensitive materials to achieve humidity measurement [5]. The explanation is that the light propagation follows the total reflection principle and this contributes to an immunity from the environment for the propagating waves. To date, there are a large amount of available sensing material enables the development of optical humidity sensor [6].

Zinc tin oxide (ZTO) is a perovskite structured nanomaterials with a wide bandgap of ~3.6 eV and outstanding optical property. By doping with other elements, the ZTO is expected to improve its optical property. Up to now, ytterbium (Yb), tantalum (Ta), and antimony (Sb) are some of the elements that have been investigated [7–9]. Ni doping may be suitable with ZTO due to its Ni^{2+} can easily occupy the Sn^{4+} because of their close ionic radii: Ni^{2+} = 0.6 Å and Sn^{4+} = 0.7 Å. Also, the doping level decreases the electron density and increases the oxygen vacancies, which enhances the sensitivity greatly [10,11]. In addition, Ni doping can improve the response recovery characteristic, repeatability, selectivity and long-term stability of sensor devices [12]. Several studies have reported on Ni doping for humidity sensing applications, such as Ni–SnO [10,13], and Ni–ZnO [14]. Despite these studies, it would be interesting

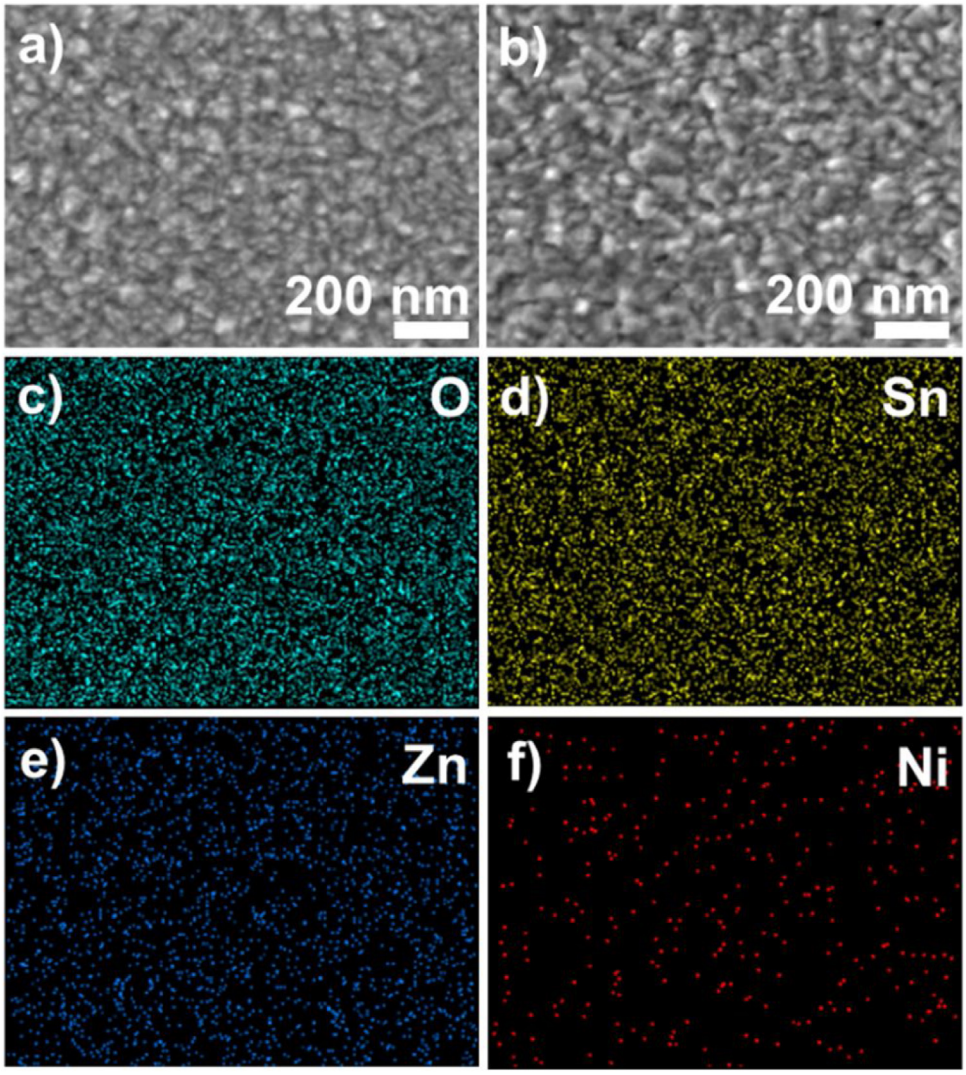

Fig. 2 – FESEM images of (a) ZTO and (b) NZTO, and elemental mapping (c) O, (d) Sn, (e) Zn and (f) Ni.

to give more insight into the application of NZTO for humidity sensing. So far, atomic layer deposition [15], pulsed laser deposition [16], and radio-frequency (RF) sputtering [17–19] are reported techniques for the deposition of ZTO thin film. All of these methods vary in terms of cost, time, and quality of the deposited films. The AACVD method is a viable simple and low-cost option. In AACVD, the precursor solution in a flask that is nebulized by the aerosol generator is directly deposited on the heated substrates to form a thin film. The composition and structure of materials can be simply controlled by the dopant, deposition time, temperature, and flow rate [20–22].

In this study, we investigate the optical reflection response of NZTO and applied for humidity sensing. The NZTO was directly deposited on the surface of borosilicate glass using AACVD. Prior to sensor testing, the optical reflection cavity was optimized by controlling the cavity length between NZTO and SMF.

2. Methodology

2.1. *Preparation of NZTO using AACVD*

All chemical was purchased from Sigma Aldrich without any further purification. The arrangement of the AACVD system used in this experiment was identical to that of another work reported elsewhere [23]. First, the equimolar concentration of $SnCl{\cdot}H_2O$ and $Zn(CH_3COO)_2{\cdot}2H_2O$ were dissolved in methanol (30 mL). Then, $Ni(CH_3COO)_2{\cdot}2H_2O$ (2 mol%) was added as a dopant in the main precursor solution. The resulting mixture was stirred at room temperature for 15 min to form a clear mixture. Borosilicate glass substrates was cut into 2×3 cm rectangles and each of the substrates were ultrasonically cleaned using detergent, de-ionized (DI) water, acetone, and 2-propanol for 10 min at each step. The substrates were placed on the hot plate and heated at 400 °C. The precursor

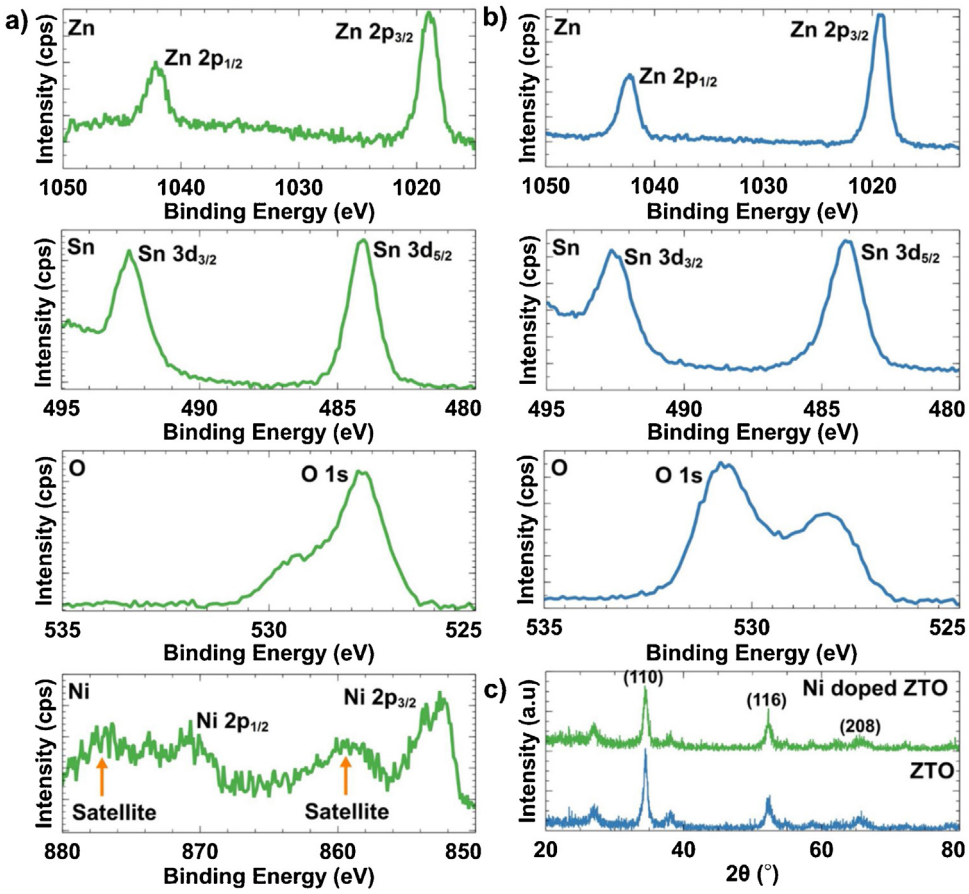

Fig. 3 – XPS spectra of (a) NZTO (green line) and (b) ZTO (blue line), and (c) XRD pattern analysis.

solution was filled in a two-neck flask. An ultra-sonic humidifier was placed under two-neck flask to generate precursor aerosols. During the deposition, the precursor aerosol was directed to the three-neck flask filtration chamber with help of carrier gas. The larger size aerosols precipitated and were filtered out, while lighter aerosols proceeded to the substrates. The carrier gas used to facilitate the movement of aerosol was purified air only. The deposition was done for 30 min. After the deposition, the samples were left cool to ambient before being tested.

2.2. *Experimental and humidity sensing setup*

Fig. 1(a) displays the experimental setup of the proposed optical reflection cavity. The cavity consists of end-cleaved SMF that directly spliced with circulator. The NZTO glass was placed in front of SMF and the distance between NZTO and SMF was adjusted using a 3-axis stage with the aid of a microscope (Dino-Lite, AM3113T) to precisely observe and measured the cavity length (see Fig. 1(b)). An amplified spontaneous emission (ASE; FiberLabs Inc, FL7004) with wavelength range of 1530–1610 nm was used as a light source. The light was launched into the cavity through a 3-port circulator and the reflection signal by the NZTO was collected by an optical spectrum analyzer (OSA; Yokogawa, AQ370B) with a resolution of 0.02 nm. The length SMF to NZTO was vary to study the optical reflection. Therefore, FSR and E_R at different length was optimized to improve operating range of the sensor before testing in humidity environment.

For humidity sensing, the setup consists of a humidity chamber (17 × 17 × 12 cm), a hygro-thermometer, and an optical reflection cavity that was placed inside the chamber. A small dish filled with known amount of NaOH pellets dissolved in DI water was placed inside the chamber, to produce moisture. During the experiments, the temperature inside the chamber was held at a constant 26 °C, consistent with the temperature outside of the chamber. A hygro-thermometer was used to measure the humidity inside the chamber, and temperature inside the chamber and surroundings, respectively. Reflection response spectrum was obtained in every 5 % increase in humidity. The setup for humidity sensing is shown in Fig. 1(c). The sensing performance was investigated by analysing the sensitivity and can be calculated by using the following Eq. (1):

$$Sensitivity = \left| \frac{\lambda_{final} - \lambda_{initial}}{RH_{final} - RH_{initial}} \right| \quad (1)$$

where λ_{final} and $\lambda_{initial}$ are the final and initial of shifted wavelength in the presence of humidity. RH_{final} and $RH_{initial}$ are the final and initial relative humidity. The unit of the calculated sensitivity is nm/RH%.

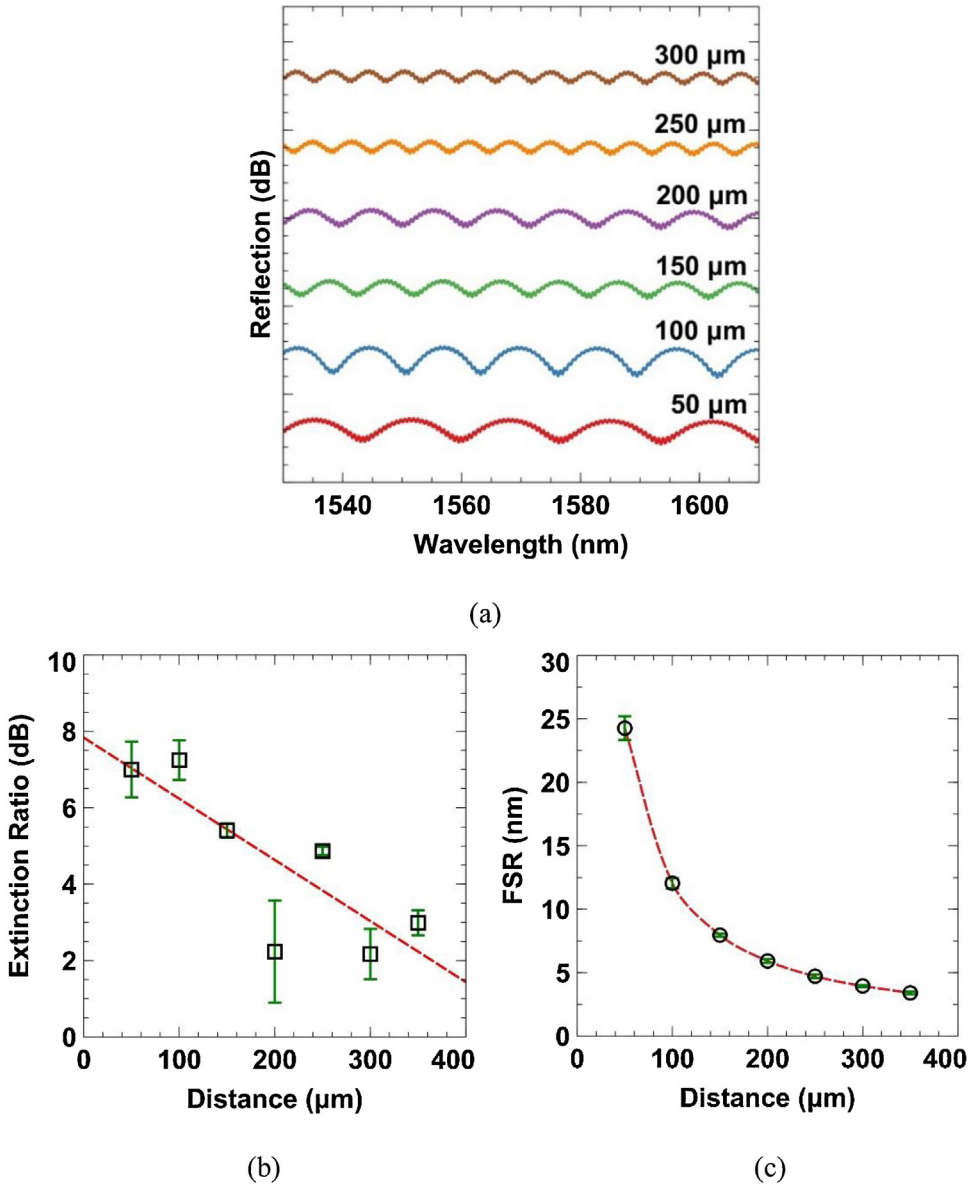

Fig. 4 – OSA trace of (a) reflection spectrum, and calculated (b) FSR and (c) E_R at different cavity length between NZTO and SMF.

3. Results and discussions

3.1. *Material characterizations*

The surface morphology of ZTO and NZTO was captured using field-emission scanning electron microscopy (FESEM; Zeiss, Supra 55-VP) at 30 kX magnification as displayed in Fig. 2(a) and (b). Looking at the images, the particle was uniformly and highly distributed throughout the glass. Both of the sample exhibit the almost similar morphology and most of the particle sizes is around 78 nm; however, the specific change in particle sizes is difficult to examine was inclusive. Therefore, elemental mapping from FESEM was conducted to identify the presence of Ni. Fig. 2(c)–(f) shows the compositional distribution of oxygen (O), tin (Sn), zinc (Zn), and Ni elements using electron X-ray dispersive spectroscopy (EDS). The elemental mapping shows that the high dense cluster of O, Sn, and Zn proves the homogenous distribution of the element and low dense cluster verifies the coexistence of Ni. Such mapping behavior results indicate that the NZTO was deposited successfully on the glass.

The composition of NZTO was further investigated by using X-ray photoelectron spectroscopy (XPS; Shimadzu, Axis Nova) as depicted in Fig. 3(a)–(b). The Zn element for both ZTO and NZTO was located at a similar peak binding energy at around 1019 eV (Zn $2p_{1/2}$) and 1043 (Zn $2p_{3/2}$). The Zn spectrum was observed to have more noise, rough peaks, and slight fluctuations for NZTO. Still, no changes and shifting in binding energy. The Sn element shows the major peak of 484 eV (Sn $3d_{3/2}$) and 492 eV (Sn $3d_{5/2}$), also no peak shifting was detected. Meanwhile, a single peak of O 1s was observed at 528 eV for NZTO;

though for ZTO, another peak was detected around 531 eV at the shoulder peak of 528 eV. It seems possible that the presence of Ni has to minimize the O vacancy in the structure. Lastly, the binding energy assigned at 872 eV (Ni $2p_{1/2}$) and 853 eV (Ni $2p_{3/2}$), proves that the Ni element is present. The binding energy positions are closely similar to the reported values of NiO [24] and are quite different from that Ni and Ni_2O_3 shows that Ni is present in a chemical state of 2^+, not as 3^+ and 0 [23,25]. The satellite peaks are also observed in the spectrum indicates that Ni is present in an oxygen environment. Ni may be incorporated in the ZTO crystallite as interstitial or substitution impurities [24,26].

Fig. 3(c) shows the X-ray diffraction (XRD; Bruker, D8 Advance) for NZTO. The material had a rhombohedral perovskite structure with parameters a = 5.2835 Å and c = 14.0913 Å with R-3 group (PDF-01-089-0095). The three major diffraction peaks are indexed to the (110), (116) and (208) planes. The (110) peaks located around 37° shifted to the slightly higher as Ni is present. The right-shifting of (110) peak means the lattice size is reducing as Ni were incorporated into the ZTO lattice. This result is likely to the related Ni^{2+} cations have a slightly smaller ionic radius (0.6 Å) when substituting the Sn^{2+} ions (0.7 Å). Hence with the smaller cations being incorporated in the ZTO lattice, its lattice size contracted [25,27]. The decline of peaks in (116) and (208) planes specifies that the crystallite size reduces gradually with the presence of Ni [25,27]. The reduction is in accord with the shifting of the pattern.

3.2. *Sensing performance*

Fig. 4(a) shows the reflection pattern of the cavity with different lengths of 50, 100, 150, 200, 250, 300, and 350 μm, respectively. What stands out in this Fig. 4(a) as the SMF moves further from the NZTO glass, the separation between the adjacent fringes was increased and more fringes appeared in the reflection spectrum. In addition, when the SMF completely touched the NZTO surface, no modulation of interference fringes was detected due to no apparent optical path difference is generated [26,28]. The reflection fringes, as a result of multiple reflections of the beam in the cavity by input and reflected light [27,29]. In the cavity, the SMF is serving as a light propagating medium where a certain amount of the propagating light is reflected at the surface of NZTO. The reflection from the NZTO was combined with the input light to produce interference fringes [26]. However, when the SMF starts to displace at a certain distance, the optical path difference is caused to vary from the original stationary position and this results in an optical phase variation.

For humidity sensing, the appropriate length was optimized based on analyzing the FSR and E_R as shown in Fig. 4(b) and (c). The FSR becomes smaller, decreasing from 24.27 nm to 3.39 nm as the distance length increases. Too small FSR will limit the operating range of the sensor and more difficult to distinguish the dipping shifting position, thus a large FSR is preferable [28,30]. Also, a cavity length of 100 μm shows the highest E_R of 7.247 dB with an FSR of 12.05 nm. Therefore, the cavity length should be balanced for designing a humidity sensing probe. The optimized cavity length is 100 μm. Fig. 5(a) and (b) shows the reflection spectrum and wavelength shifting at different humidity. When the humidity increase from 60 to 90 %, the dipping shifts from 1546.1 to 1537.9 nm. No change in FSR and E_R was observed, shows that the presence of humidity only shifting the reflection wavelength. The reflection spectrum with respect to humidity can be explained based on the adsorption mechanism of water molecules [31,32]. The Ni^{2+} presence in ZTO lattice form defective energy level and introduce rich oxygen vacancies and thus the chemisorption and physisorption improves [14]. When NZTO was exposed to the humid environment, the water molecules were chemisorbed with Ni^{2+} of ZTO creates a strong electrostatic field and then first hydroxyl layer physisorption of water molecules was absorbed through double hydrogen bonding. As the humidity increase, second hydroxyl layer was further formed through the action of single hydrogen bonding resulting in an increased dielectric constant, which in turn change the effective refractive index and modulate the reflection of light on the surface of NZTO [33–35].

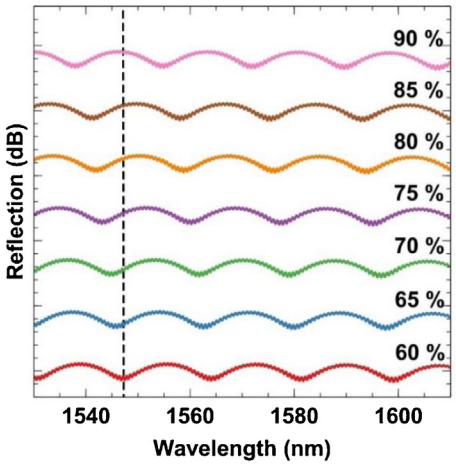

(a)

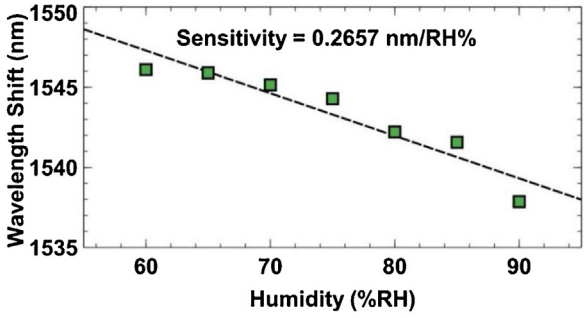

(b)

Fig. 5 – OSA trace of (a) Reflection spectrum and (b) sensitivity at different humidity of 60–90%.

4. Conclusion

In conclusion, we have demonstrated a humidity sensing based on NZTO perovskite thin film as a sensing material for improved sensitivity and optical performance. The NZTO was deposited on borosilicate glass substrate using AACVD and Ni dopant with 2 %mol was used into the precursor solution

of ZTO. The optical performance was investigates using the optical reflection cavity and evaluates from the FSR and E_R. The cavity was made by placing the SMF at the in front of NZTO and SMF was adjusted at x-direction to obtain different cavity length. The best cavity length obtained is 100 μm with FSR and E_R of 12.05 nm and 7.247 dB. Also, 100 μm was selected for humidity sensing by inserting the cavity inside the humidity chamber. The results show that the reflection spectrum was blue-shifted from 1546.1 to 1537.9 nm as humidity increased. The sensitivity of the proposed sensor is 0.2657 nm/RH% shows that it has potential in optical humidity sensing application.

Conflicts of interest

The author declares no conflicts of interest.

Acknowledgements

This work was supported by Universiti Kebangsaan Malaysia [DIP-2018-002] and Universiti Teknologi Malaysia [UTMHR, 2243.08G99].

REFERENCES

[1] Lakhiar IA, Jianmin G, Syed TN, Chandio FA, Buttar NA, Qureshi WA. Monitoring and control systems in agriculture using intelligent sensor techniques: a review of the aeroponic system. J Sens 2018;2018:8672769.
[2] Zambrano MV, Dutta B, Mercer DG, MacLean HL, Touchie M. Assessment of moisture content measurement methods of dried food products in small-scale operations in developing countries: a review. Trends Food Sci Technol 2019;88:484–96.
[3] Mardonova M, Choi Y. Review of wearable device technology and its applications to the mining industry. Energies 2018;11(3):547.
[4] Ascorbe J, Corres JM, Arregui FJ, Matias IR. Recent developments in fiber optics humidity sensors. Sensors 2017;17(4):893.
[5] Liu Y, Li P, Zhang N, Zhang X, Chen S, Liu Z, et al. Fiber-optic evanescent field humidity sensor based on a micro-capillary coated with graphene oxide. Opt Mater Express 2019;9(11):4418–28.
[6] Kolpakov SA, Gordon NT, Mou C, Zhou K. Toward a new generation of photonic humidity sensors. Sensors 2014;14(3):3986–4013.
[7] Oh SH, Ferblantier G, Park YS, Schmerber G, Dinia A, Slaoui A, et al. Low-temperature growth and electronic structures of ambipolar Yb-doped zinc tin oxide transparent thin films. Appl Surf Sci 2018;441:49–54.
[8] Cai S, Li Y, Chen X, Ma Y, Liu X, He Y. Optical and electrical properties of Ta-doped $ZnSnO_3$ transparent conducting films by sol–gel. J Mater Sci Mater Electron 2016;27(6):6166–74.
[9] Fei C, Qiu H, Ming L, Zhou H, Yu L, Min C, et al. Sb doped $ZnSnO_3$ transparent and conducting thin films: preparation and property. Chin J Inorg Chem 2016;30(5):1212–20.
[10] Manikandan V, Petrila I, Vigneselvan S, Mane RS, Vasile B, Dharmavarapu R, et al. A reliable chemiresistive sensor of nickel-doped tin oxide (Ni–SnO_2) for sensing carbon dioxide gas and humidity. RSC Adv 2020;10(7):3796–804.
[11] Zhang D, Cao Y, Yang Z, Wu J. Nanoheterostructure construction and DFT study of Ni-doped In_2O_3 nanocubes/WS_2 hexagon nanosheets for formaldehyde sensing at room temperature. ACS Appl Mater Interfaces 2020;12(10):11979–89.
[12] Zhang D, Wu J, Li P, Cao Y. Room-temperature SO_2 gas-sensing properties based on a metal-doped MoS_2 nanoflower: an experimental and density functional theory investigation. J Mater Chem A 2017;5(39):20666–77.
[13] Ibrahim NB, Arsad AZ, Yusop N, Baqiah H. The physical properties of nickel doped indium oxide thin film prepared by the sol-gel method and its potential as a humidity sensor. Mater Sci Semicond Process 2016;53:72–8.
[14] Sun N, Ye Z, Kuang X, Liu W, Li G, Bai W, et al. High sensitivity capacitive humidity sensors based on $Zn_{1-x}Ni_xO$ nanostructures and plausible sensing mechanism. J Mater Sci Mater Electron 2019;30(2):1724–38.
[15] Heo J, Kim SB, Gordon RG. Atomic layer deposited zinc tin oxide channel for amorphous oxide thin film transistors. Appl Phys Lett 2012;101(11):113507.
[16] Schlupp P, von Wenckstern H, Grundmann M. Schottky barrier diodes based on room temperature fabricated amorphous zinc tin oxide thin films. Phys Status Solidi A 2017;214(10):1700210.
[17] Frenzel H, Dörfler T, Schlupp P, von Wenckstern H, Grundmann M. Long-throw magnetron sputtering of amorphous Zn–Sn–O thin films at room temperature. Phys Status Solidi A 2015;212(7):1482–6.
[18] McDowell MG, Sanderson RJ, Hill IG. Combinatorial study of zinc tin oxide thin-film transistors. Appl Phys Lett 2008;92(1):013502.
[19] Min SY, Cho WJ. Rare metal-free high-performance zinc–tin oxide thin film transistors using efficient energy conversion of microwave annealing. Phys Status Solidi A 2020;217(12):1900997.
[20] Noh MFM, Soh MF, Teh CH, Lim EL, Yap CC, Ibrahim MA, et al. Effect of temperature on the properties of SnO_2 layer fabricated via AACVD and its application in photoelectrochemical cells and organic photovoltaic devices. Sol Energy 2017;158:474–82.
[21] Noh MFM, Soh MF, Riza MA, Safaei J, Nasir SNF, Sapian NWM, et al. Effect of film thickness on photoelectrochemical performance of SnO_2 prepared via AACVD. Phys Status Solidi A 2018;255(6):1700570.
[22] Dixon SC, Jiamprasertboon A, Carmalt CJ, Parkin IP. Luminescence behaviour and deposition of Sc_2O_3 thin films from scandium(III) acetylacetonate at ambient pressure. Appl Phys Lett 2018;112(22):221902.
[23] Sialvi MZ, Mortimer RJ, Wilcox GD, Teridi MAM, Varley TS, Wijayantha KU, et al. Electrochromic and colorimetric properties of nickel(II) oxide thin films prepared by aerosol-assisted chemical vapor deposition. Appl Mater Interfaces 2013;5(12):5675–82.
[24] Grosvenor AP, Biesinger MC, Smart RSC, McIntyre NS. New interpretations of XPS spectra of nickel metal and oxides. Surf Sci 2006;600(9):1771–9.
[25] Rambu AP, Ursu L, Iftimie N, Nica V, Dobromir M, Iacomi F. Study on Ni-doped ZnO films as gas sensors. Appl Surf Sci 2013;280:598–604.
[26] Ghosh S, Srivastava P, Pandey B, Saurav M, Bharadwaj P, Avasthi DK. Study of ZnO and Ni-doped ZnO synthesized by atom beam sputtering technique. Appl Phys A 2008;90(4):765–9.
[27] Kumar AA, Kumar AA, Quamara JK, Dillip GR, Joo SW, Kumar J. Fe(III) induced structural, optical, and dielectric behavior of cetyltrimethyl ammonium bromide stabilized strontium stannate nanoparticles synthesized by a facile wet chemistry route. RSC Adv 2015;5(22):17202–9.
[28] Seat HC, Pullteap S. An extrinsic fiber Fabry–Perot interferometer for dynamic displacement measurement. In:

International Conference on Mechatronics and Automation. 2007. p. 3025–30.
[29] Chen M, Xie S, Zhou G, Wei D, Wu H, Takahashi S, et al. Absolute distance measurement based on spectral interferometer using the effect of the FSR of a Fabry–Perot etalon. Opt Lasers Eng 2019;123:20–7.
[30] Li J, Yang J, Ma J. Highly sensitive temperature sensing performance of a microfiber fabry-perot interferometer with sealed micro-spherical reflector. Micromachines 2019;10(11):773.
[31] Farahani H, Wagiran R, Hamidon MN. Humidity sensors principle, mechanism, and fabrication technologies: a comprehensive review. Sensors 2014;14(5):7881–939.
[32] Weng Z, Qin J, Umar AA, Wang J, Zhang X, Wang H, et al. Lead-free $Cs_2BiAgBr_6$ double perovskite-based humidity sensor with superfast recovery time. Adv Funct Mater 2019;29(24):1902234.
[33] Zhang D, Wang D, Li P, Zhou X, Zong X, Dong G. Facile fabrication of high-performance QCM humidity sensor based on layer-by-layer self-assembled polyaniline/graphene oxide nanocomposite film. Sens Actuators B Chem 2018;255:1869–77.
[34] Zhang D, Sun YE, Li P, Zhang Y. Facile fabrication of MoS_2-modified SnO_2 hybrid nanocomposite for ultrasensitive humidity sensing. ACS Appl Mater Interfaces 2016;8(22):14142–9.
[35] Harith Z, Irawati N, Rafaie HA, Batumalay M, Harun SW, Nor RM, et al. Tapered plastic optical fiber coated with Al-doped ZnO nanostructures for detecting relative humidity. IEEE Sens J 2014;15(2):845–9.